



Cite this: DOI: 10.1039/c8cp04964e

Nucleation of pseudo hard-spheres and dumbbells at moderate metastability: appearance of A15 Frank–Kasper phase at intermediate elongations

 Itziar Zubieta,^a Miguel Vázquez del Saz,^{ab} Pablo Llombart,^a Carlos Vega^b and Eva G. Noya  ^{*a}

Crystal nucleation of repulsive hard-dumbbells from the sphere to the two tangent spheres limit is investigated at moderately high metastability by brute-force molecular dynamics simulations. Nucleation rates are in good agreement with previous simulations of hard-spheres and dumbbells. Icosahedral structures formed by twinned face-centred-cubic tetrahedra sharing five-fold symmetry axes and icosahedral centers are often found in spheres and dumbbells with either small ($L/\sigma = 0.1$ and 0.2) and large ($L/\sigma = 1$) elongations. These structures are incompatible with long range crystalline order but are able to survive up to quite large sizes. In contrast, at intermediate elongations ($L/\sigma = 0.3$), corresponding roughly to the bond length of molecular nitrogen, the fluid crystallizes into three distinct solid structures, namely, a low density plastic crystal, a hexagonal close-packed plastic crystal (with the same structure as β -N₂), and an A15 Frank–Kasper phase (cP8 structure corresponding to δ -N₂). At the lower pressures studied the hexagonal close packed plastic crystal is the most stable phase, but at the higher pressures the stable phase is an orientationally ordered solid designated as CP1 that is never spontaneously formed in our crystallization simulations.

Received 4th August 2018,
Accepted 12th October 2018

DOI: 10.1039/c8cp04964e

rsc.li/pccp

1 Introduction

Understanding the nucleation and growth of crystals from the fluid phase is a fundamental issue with important implications in many fields, such as, for example, in pharmaceutical, atmosphere or material sciences. However, in spite of much experimental, theoretical and simulation efforts, the mechanism of crystal nucleation is far from being completely understood.¹ This is true even for the simplest molecular models, such as hard-spheres (HS). Crystallization of HS was predicted by molecular simulation in the pioneering works of Alder and Wainwright² and Wood and Jacobson³ in the fifties, and experimentally demonstrated in the eighties.⁴ HS have been often used as the model of reference to study the fundamentals of crystal nucleation,⁵ but still there are many aspects related to their nucleation that are lively debated in the recent literature. Firstly, there is no agreement between the experimental and simulated nucleation rates.^{6–9} Secondly, the microscopic mechanism

of crystal nucleation and growth is also unclear. Schilling *et al.* argue that crystallization of hard-spheres is a two-step process in which dense amorphous nuclei form first and then these nuclei act as precursors for the emergence of crystalline order.^{10,11} From a different view, Kawasaki and Tanaka propose that nucleation takes place in transient configurations with medium size structural order.^{12,13}

While crystal nucleation of simple spherical particles has been intensively investigated, simple models that introduce shape anisotropy have received much less attention.^{8,14–16} One of the simplest models of anisotropic particles is the hard-dumbbells model (HD), which consists of two hard-spheres, each of diameter σ , with a rigid bond between them of length $L^* = L/\sigma$. This simple model can be representative of simple diatomic molecules such as nitrogen, and this motivated early studies of the phase diagram of HD with elongations between zero and one.^{17–19} More recently this system has received renewed interest^{20,21} as it is now possible to produce synthetic dumbbell-shaped colloids.^{22–29} These particles can assemble into crystals with unusual photonic properties, which make them attractive for many optical applications. But they are also interesting from a fundamental point of view, as dumbbell-shaped colloids can be used to experimentally investigate the effect of shape anisotropy on

^a Instituto de Química Física Rocasolano, Consejo Superior de Investigaciones Científicas, CSIC, Calle Serrano 119, 28006 Madrid, Spain.

E-mail: eva.noya@gmail.com; Fax: +34 915642431; Tel: +34 915619400

^b Departamento de Química Física (Unidad Asociada de I+D+i al CSIC), Facultad de Ciencias Químicas, Universidad Complutense de Madrid, 28040 Madrid, Spain

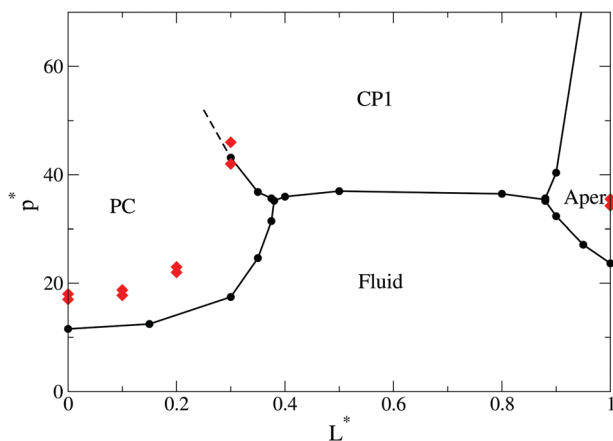


Fig. 1 Phase diagram of hard-dumbbells as a function of elongation L^* . Data were taken from ref. 18 and 20. The upper and lower pressures for each elongation at which crystallization is studied in this work are marked with red diamonds.

the crystal nucleation behaviour. In that respect, simulation studies are especially relevant to both guide and complement experiments.

In order to study the crystal nucleation behaviour of a given system, its equilibrium phase diagram must be known. Several simulation studies have addressed this topic^{17–20} and it can be stated that the phase diagram of HD is now quite well understood. A schematic representation is shown in Fig. 1. At low elongations ($L^* \leq 0.38$) the fluid freezes into a close-packed plastic crystal where the centers of mass of the molecules form an ordered lattice but they are able to rotate. Accurate estimates of the free energy showed that differences between face-centred-cubic (FCC) and hexagonal close-packed (HCP) plastic crystals are rather small, the FCC plastic being marginally more stable at low elongations but becoming metastable with respect to the HCP as elongation and pressure increase.²⁰ The close-packed (FCC or HCP) plastic crystal undergoes a second transition to an orientationally ordered solid (designated CP1 in ref. 17) at a pressure that decreases as elongation increases, so that the plastic is no longer thermodynamically stable for elongations above $L^* \approx 0.38$.¹⁸ In CP1 molecules are packed in double hexagonal layers so that each sphere also lies in a hexagonal layer, tilted by $\arcsin(L^*/\sqrt{3})$ with respect to the normal to these planes. These double layers are then stacked following an ABC sequence. The free energy of CP1 is virtually identical to that of other orientationally ordered structures, named CP2 and CP3. CP2 differs from CP1 in the stacking of the layers (here it follows an AB sequence), whereas the difference in CP3 arises from the tilt angle (in CP3 it alternates between adjacent layers). The fluid freezes directly into an orientationally ordered solid at intermediate elongations, whereas at elongations close to one it forms an aperiodic solid in which dumbbells are orientationally disordered but disposed in such a way that each sphere lies in the lattice positions of a close-packed structure. This aperiodic crystal is entropically favoured over CP1 (due to its high configurational entropy) but is destabilized as pressure increases. Thus there is a second

transition from the aperiodic to the CP1 solid at a pressure that increases with elongation. Given that dumbbells with $L^* \approx 0.3$ can be seen as a simplified model of molecular nitrogen, early studies considered also the stability of α -N₂ structure (the centers of the molecules are arranged in an FCC lattice and their axes are oriented along the diagonals of the cubic cell). For HD, this phase is thermodynamically unstable, but mechanically stable for $L^* = 0.3$ at high pressure, and for $L^* = 0.6$ at moderate pressure.¹⁷

Besides the equilibrium phase behaviour, crystal nucleation of HD has also already been investigated by molecular simulations.²¹ This study was restricted to the plastic phase at low elongation and the aperiodic crystal at high elongations, as crystallization of the orientationally ordered solid (at intermediate elongations) was found to be strongly hindered by a high free energy barrier at low supersaturations and by an extremely slow dynamics at high supersaturations. For the plastic crystal, the nucleation rate (measured in long-diffusion times to exclude the effect of dynamics) decreases with elongation (due to a slight increase of the free energy barrier) at low supersaturation, but remains virtually constant at high supersaturation (the free energy barrier decreases and dynamics becomes slower). For the aperiodic crystal, the nucleation rate increases for shorter elongations due to the decrease of the nucleation barrier. Finally they also showed that the plastic crystal nucleus was made of mainly FCC particles at low elongation, and by HCP particles at elongations above $L^* \approx 0.2$, which is consistent with the fact that the HCP crystal becomes stable above $L^* \approx 0.15$. With regard to the aperiodic crystal, the nucleus consists mainly of FCC-like particles.

One aspect of nucleation of HD that is particularly interesting and that has not yet been explored in previous work concerns the crystallization of dumbbells with elongations close to the disappearance of the plastic ($L^* = 0.3$ – 0.35) and aperiodic phases ($L^* = 0.9$ – 0.95) at pressures in the neighbourhood of the transition to the orientationally ordered solid. Under those conditions, there is a competition between orientationally disordered phases (plastic at low elongations and aperiodic crystal at large elongations) and the orientationally ordered solid (CP1) that is likely to lead to an interesting crystallization behaviour. In particular, consistent with Ostwald's observation,³⁰ it is not unexpected to find that the phase that nucleates first does not coincide with the thermodynamically stable phase. According to classical nucleation theory,³¹ the nucleation rate is related to the free energy barrier for the formation of a critical nucleus in the fluid through $J \propto \exp - (\Delta G/k_B T)$. Stranski and Totomanow rationalized Ostwald's observation by stating that the phase that forms first is that separated from the fluid by a lower free energy barrier, ΔG .³² In view of this, one of the aims of this work is to revisit the problem of HD nucleation.

Due to computational reasons, we modelled the spheres in the dumbbells using a continuous version of HS, designated as the pseudo-hard sphere model (PHS).³³ This model has been shown to reproduce closely the properties of HS over a broad range of thermodynamic conditions.^{33–35} Given that all the previous work was done for HD,²¹ we performed extensive

brute-force simulations of the nucleation at low elongations ($L^* = 0, 0.1, \text{ and } 0.2$) and high elongations ($L^* = 1.0$) that prove that the crystallization behaviour of the pseudo-hard dumbbells (PHD) is very similar to that of HD. Then, the nucleation behaviour of PHD with $L^* = 0.3$ is studied at pressures slightly below and above the coexistence of the plastic and orientationally ordered solids ($p^* = 43.13^{18}$). This pressure corresponds to a high supersaturation (as measured by the difference in chemical potential between the solid and fluid phases), which makes it possible to study nucleation by (lengthy) brute-force simulations. Besides their simplicity, brute-force simulations have the advantage that, as they are not biased, the system can evolve into any crystal structure, being that coincident or not with one of the expected solid phases. As mentioned before, the choice of dumbbells $L^* = 0.3$ is also particularly interesting as this elongation is rather close to that of molecular nitrogen. Thus our findings might contribute to better understand the effect of shape on the behaviour of molecular nitrogen.

2 Simulation details

In this work we investigate the nucleation of spheres and dumbbells with elongations $L^* = 0-1$ by means of unbiased brute force simulations. Molecular Dynamics (MD) simulations in the NpT ensemble were carried out with the GROMACS 5.1 simulation package.^{36,37} As it is not possible to simulate discontinuous potentials with GROMACS, we used the continuous PHS model recently proposed by Jover *et al.*³³ This model has been shown to exhibit virtually the same behaviour as HS at $T^* = kT/\varepsilon = 1.5$ both in equilibrium and in the metastability region.³³⁻³⁵ In particular, both models predict very similar nucleation rates in a broad metastability range.³⁸ For its implementation in GROMACS the model parameters were assigned values corresponding to argon ($\sigma = 3.405 \text{ \AA}$, $\varepsilon/k_B = 117.87 \text{ K}$ and $m = 39.946 \text{ u}$), although results will be presented in reduced units $\rho^* = \rho d^3$, $T^* = kT/\varepsilon$, $p^* = p d^3/kT$ and $t^* = t \sqrt{k_B T / (m \sigma^2)}$, where d is the diameter of a sphere with the same volume as the dumbbell ($d^3 = \sigma^3(1 + 3/2L^* - 1/2L^{*3})$). Even though for soft models the packing fraction is not strictly defined, given the high similarity between PHD and HD, the common definition of packing fraction $\eta = \rho^* \pi/6$ is adopted here. The equations of movement were integrated using a time step of 0.002 ps. Temperature was controlled using a velocity rescaling with a stochastic term³⁹ and pressure using a Parrinello–Rahman barostat.⁴⁰ A system size of $N = 8000$ molecules was used to study nucleation, whereas simulations of the equation of state were performed using a smaller system size of $N \approx 500$. As can be seen in Fig. 2, dumbbells made of two PHS reproduce quite closely the equation of state of the fluid and solid phase CP1 of HD at several elongations ($L^* = 0.3, 0.6$ and 1). In view of this and the similarity between all the properties between HS and PHS, it is likely that PHD and HD also present very similar crystallization behaviour. Curiously, the reduced density of the CP1 solid is almost identical for dumbbells with $L^* = 0.3$ and $L^* = 0.6$ for a certain reduced pressure.

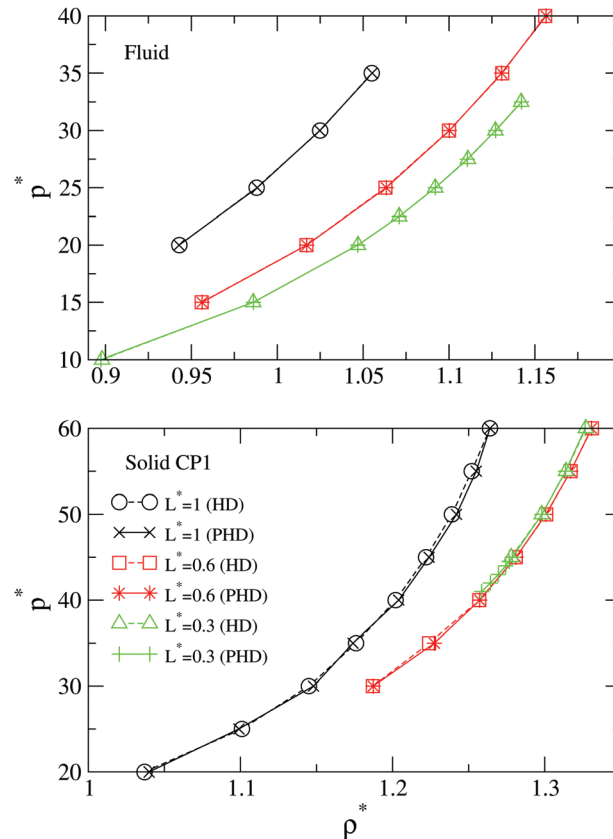


Fig. 2 Comparison of the evolution of density of the fluid and solid CP1 phases for HD and PHD with $L^* = 1, 0.6$ and 0.3 .

For $L^* = 0$, *i.e.* for the limit case of spheres, we also performed event-driven MD simulations of the HS model using a home-made code.⁴¹ The aim of these simulations was to assess the impact of using the PHS instead of the HS model. In this case, simulations were carried out in the NVE ensemble at a packing fraction of 0.5393 that corresponds roughly to a reduced pressure of about $p^* = 17.5$.⁴²

Crystal nucleation and growth was monitored by following the evolution of the number of solid particles within the fluid. In NpT simulations, crystallization is also usually signaled by an abrupt increase of density. Particles were identified as solid or liquid using the local averaged order parameters proposed by Lechner and Dellago.⁴³ The molecular centers of mass were used for the evaluation of the order parameters of PHD with $L^* = 0-0.3$, whereas the position of each sphere in the dumbbell was considered for PHD with $L^* = 1$. Two particles were considered first neighbours if the distance between them was lower than that of the first minimum in the radial distribution function of the solid. As can be seen in Fig. 3, \bar{q}_6 is able to discriminate between fluid and solid particles and \bar{q}_4 HCP from FCC environments. The limiting values that separate fluid from solid and FCC from HCP environments for each elongation are provided in Table 1. Once that particles have been identified as solid-like or liquid-like, the size of the largest solid cluster was followed using a cluster analysis algorithm.⁴⁴

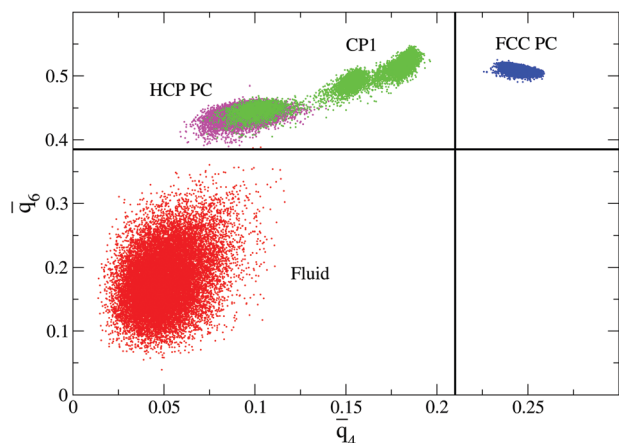


Fig. 3 Map of the order parameters \bar{q}_6 vs. \bar{q}_4 for the fluid, HCP, and FCC plastic crystal phases for dumbbells with $L^* = 0.3$ at $p^* = 43$. The black lines mark the \bar{q}_6 and \bar{q}_4 limits to distinguish between the fluid and the solid, and between HCP and FCC environments.

Table 1 Values of \bar{q}_6 and \bar{q}_4 used to discriminate fluid from solid, and HCP from FCC environments, respectively, at different L^* . The cutoff used to define two molecules as first neighbours is also provided. Molecules with $\bar{q}_6 > \bar{q}_{6,\text{limit}}$ are labelled as solid and molecules with $\bar{q}_4 > \bar{q}_{4,\text{limit}}$ are labelled as FCC

L^*	r_c^*	$\bar{q}_{4,\text{limit}}$	$\bar{q}_{6,\text{limit}}$
0	1.32	0.140	0.400
0.1	1.44	0.125	0.380
0.2	1.44	0.132	0.360
0.3	1.44	0.210	0.385
1.0	1.32	0.140	0.410

The nucleation rate J is defined as

$$J = \frac{1}{\langle t \rangle V}, \quad (1)$$

where $\langle t \rangle$ is the average time for nucleation, calculated as the time at which the number of solid particles increases rapidly (which in NpT simulations coincides with an abrupt increase in the system density) and V is the simulation box volume. It is important to stress that the use of this expression is only strictly valid if only one nucleus forms. When the crystal grows from two or more nuclei, this fact should be taken into account, making the estimation of the nucleation rate more difficult. Thus, our study was restricted to pressures in which nucleation occurs from one single cluster. With the aim of excluding dynamic effects it is common to express this magnitude in long diffusion times: $\tau_D = \sigma^2 / (6D_f)$, D_f being the diffusion constant of the fluid. Typically ten independent crystallization simulations were performed at each pressure and elongation, but in some cases this number was increased to twenty to get better statistics.

Unbiased brute-force simulations do not allow us to get an accurate estimate of the nucleation free energy barrier ΔG . That will require the use of special simulation techniques such as umbrella sampling.⁵ However a rough estimation can be

obtained by using the relation between J and ΔG provided by the classical nucleation theory,³¹

$$J = Zf^+ \rho_f \exp\left(-\frac{\Delta G}{k_B T}\right) \quad (2)$$

where Z is the Zeldovich factor, related to the curvature of the free energy profile at the top of the free energy barrier and which is given within classical nucleation theory as $Z = \sqrt{\Delta\mu / (6\pi k_B T N_c)}$, f^+ is the attachment rate and ρ_f is the density of the fluid phase. Here N_c is the number of particles of the critical nucleus and $\Delta\mu$ is the chemical potential difference between the fluid and solid phases. The attachment rate can be estimated from $f^+ = 24DN_c^{2/3}/\lambda^2$, where λ is of the order of the molecular diameter.^{38,45}

As a consequence of using unbiased simulations, our study is limited to a rather narrow window of pressures corresponding to moderately high supersaturations. At lower moderate supersaturations nucleation barriers are too high and nucleation is a rare event which will virtually never be seen in unbiased simulations. In contrast, at high supersaturations the nucleation barrier becomes so small that multiple clusters appear but their growth is severely hampered by the slow dynamics of the system.⁴⁵ As mentioned before, the formation of more than one cluster is not desirable as it makes it more difficult to estimate the nucleation rate from eqn (1).

In some selected trajectories, crystallization was also monitored using a common neighbour analysis (CNA).⁴⁶ In CNA, each bond between two particles is assigned three indices, the first corresponds to the number of common neighbours to the two particles, the second gives the number of bonds within the subset of common neighbours, and the third accounts for the largest number of contiguous bonds within this set. Each solid structure has a distinctive CNA signature that can be used for crystal identification (Table 2). Although this analysis is known to be rather sensitive to small vibrations in the crystal structure that can be partially alleviated by using a variable cutoff distance to define nearest neighbours,⁴⁷ we found it to be rather useful to complement the structural analysis in some instances in which the Lechner and Dellago order parameter fails to distinguish solid from fluid particles (which often

Table 2 CNA signature of different molecular environments. In the last column, the three first numbers give the CNA signature and the number in parentheses the number of neighbours with this signature. In some structures, such as e.g. in HCP, not all the bonds formed between a central particle and its neighbours have all the same CNA signature. In these cases, the list of all CNA signatures is provided. For cP8 there are two types of positions depending on their local environment and the CNA signature for each of them is given

Environment	No. of neighbours	CNA (no. of neighbours)
FCC	12	421(12)
HCP	12	422(6), 421(6)
Icosahedral spine	12	422(6), 421(6)
Icosahedral center	12	555(12)
12-Coordinated atoms in cP8	12	555(12)
14-Coordinated atoms in cP8	14	555(12), 666(2)

occurs when the solid environment has a large degree of icosahedral order).

Besides local order parameters, global indicators can also be useful to characterize the solids formed from the melt. In particular, radial distribution functions (RDF) and bond orientational order diagrams (BOOD)⁴⁸ were used for that aim. The degree of orientational order of the molecules in the solids was assessed by calculating the probability distributions:

$$f(\theta) = \left\langle \frac{N(\theta)}{N \sin(\theta) \Delta\theta} \right\rangle \quad (3)$$

$$f(\phi) = \left\langle \frac{N(\phi)}{N \Delta\phi} \right\rangle \quad (4)$$

where θ is the angle formed by the molecular and z axes and ϕ is the angle formed by the projection of the molecular axis on the xy -plane and the x -axis. $N(\alpha)$ is the number of molecules with an angle between α and $\alpha + \Delta\alpha$, $\alpha = \theta$ or ϕ . Note that crystals must be oriented with respect to their symmetry axes prior to the evaluation of these distribution functions.

3 Results

3.1 Nucleation of PHS ($L^* = 0$)

Crystallization of PHS was investigated within the interval $p^* = 17$ –18. Nucleation events are clearly signaled by an abrupt increase of density that is correlated to a sudden enhancement of the number of particles in the largest solid cluster as identified by the Lechner and Dellago order parameter (see Fig. 4(d)). Nucleation rates are collected in Table 3 and compared with previous simulation results in Fig. 4. As can be seen, our estimates of the PHS nucleation rate at a given packing fraction are about an order of magnitude lower than those obtained for HS in previous work.^{8,49} Even though this difference is within the uncertainty in the estimation of the nucleation rate, this systematic difference motivated us to perform simulations also for the HS model. The nucleation rate calculated at a packing fraction $\eta = 0.5393$ using NVE MD simulations deviates slightly from PHS results and is in closer agreement with previous data for HS, which again indicates that there are small but appreciable differences (of about an order of magnitude) in the nucleation rates of the PHS and HS models.

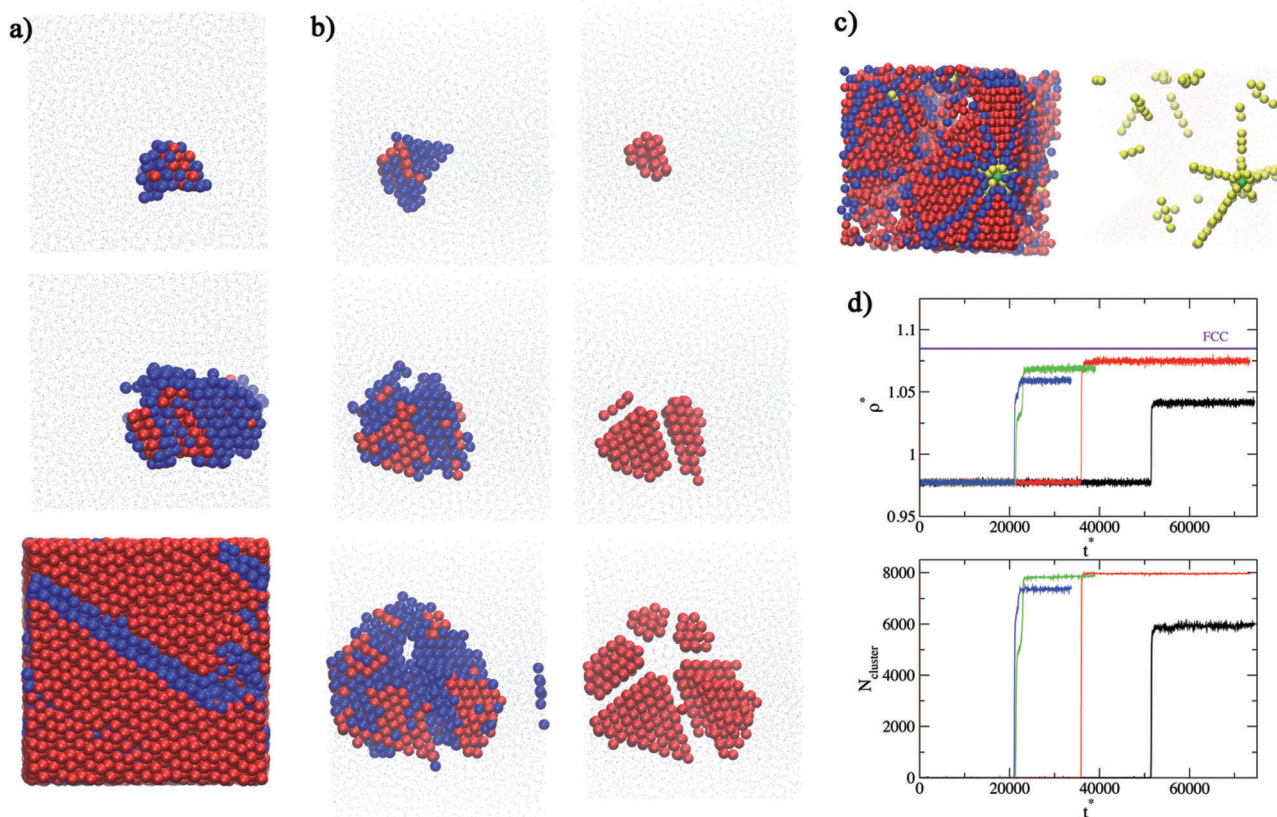


Fig. 4 (a and b) Two examples of growth of the crystal nucleus in PHS (*i.e.* $L^* = 0$) at $p^* = 17$. In (a) the system forms a layered solid, whereas in (b) it holds a twinned tetrahedral structure up to fairly large size. Particles in FCC environments are shown in red and those in HCP environments are depicted in blue (as identified with Lechner and Dellago order parameters). In (b) two different views are shown at each time, one in which both FCC and HCP are shown (left column) and other in which HCP particles, which are usually at the nucleus surface, are removed. (c) Analysis of a twinned tetrahedral structure with CNA. Besides FCC and HCP environments, particles within five-fold symmetry axes are shown in yellow and those at icosahedral centers in green. (d) Evolution of the density (upper panel) and number of solid particles (bottom panel) along selected trajectories for PHS at $p^* = 17$. The horizontal blue line shows the equilibrium density of the FCC solid.

Table 3 Nucleation rates of PHS as obtained from NpT MD simulations as a function of pressure. NVE simulations for HS at one single reduced pressure have also been performed for comparison. Nucleation rates are expressed in units of long diffusion times, $J^* = J\sigma_{\text{PHS}}^3\tau_D$

Model	p^*	η	η_{scaled}	$\langle t^* \rangle$	$D_{\text{r}}^* (\times 10^3)$	J^*
PHS	17.00	0.5361	0.5332	40 590	8.3	6.7×10^{-8}
PHS	17.25	0.5381	0.5352	21 843	7.5	1.3×10^{-7}
PHS	17.50	0.5396	0.5367	7162	7.1	4.4×10^{-7}
PHS	17.75	0.5426	0.5387	1060	6.5	3.2×10^{-6}
PHS	18.00	0.5437	0.5407	805	6.2	1.3×10^{-5}
HS		0.5393	—	1560	6.0	2.0×10^{-6}

These small differences between the nucleation rates of PHS and HS can be rationalized by considering the fact that PHS is indeed a continuous penetrable potential. Following previous work,⁵⁰ the softness of the PHS model can be accounted for by using an effective diameter which is calculated from the packing fractions of the PHS and HS fluids at the melting point. For the HS model, the fluid–solid transition occurs at $p_{\text{coex}}^{\text{HS}} = 11.54$ and the packing fractions at coexistence are $\eta_{\text{solid}}^{\text{HS}} = 0.54292$ and $\eta_{\text{fluid}}^{\text{HS}} = 0.49087$.⁵¹ These values are slightly different for the PHS model, for which $p_{\text{coex}}^{\text{PHS}} = 11.65$, $\eta_{\text{solid}}^{\text{PHS}} = 0.54440$ and $\eta_{\text{fluid}}^{\text{PHS}} = 0.49351$.³⁴ The effective diameter $\sigma_{\text{PHS,eff}}$ of the PHS model can be calculated from

$$\frac{\eta_{\text{fluid}}^{\text{HS}}}{\eta_{\text{fluid}}^{\text{PHS}}} = \frac{\sigma_{\text{PHS,eff}}^3}{\sigma_{\text{PHS}}^3} = 0.9946 \quad (5)$$

As can be seen in Fig. 5 and Table 3 when compared using the scaled packing fractions nucleation rates of PHS and HS are in much better agreement.

Coming back to the evolution of the density (Fig. 4(d)), it is interesting to note that in some trajectories the equilibrium value after the jump is appreciably lower than that of the most stable solid, whereas in others it almost reaches its bulk value.

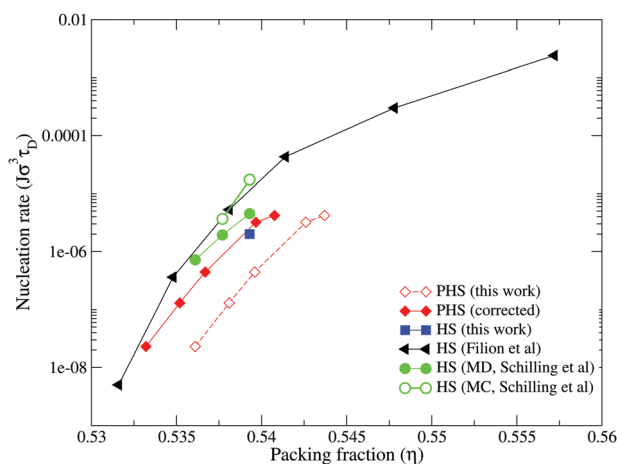


Fig. 5 Nucleation rate of HS and PHS (*i.e.* $L^* = 0$) as a function of packing fraction. For PHS two sets of data are provided: light red diamonds show the nucleation rates obtained from our simulations and dark red diamonds show corrected results that take into account the effective diameter of PHS. Simulation results taken from ref. 8 and 49 are also included for comparison.

A detailed analysis of the microscopic behaviour reveals that at early stages the crystal nucleus is formed mainly by a core of FCC particles surrounded by HCP particles located at the solid–fluid interface (see Fig. 4(a and b)). From this point the system can follow two different growth mechanisms. One of these corresponds to the usual growth path in which the nucleus grows quickly to form a large crystal (Fig. 4(a)). Usually those trajectories whose final density is close to that of the solid follow this path. In the second mechanism, occurring mainly in those trajectories that are not able to reach the solid bulk density, the interfacial HCP particles promote the formation of twinned FCC tetrahedra joined by HCP planes and sharing an edge that constitutes a five-fold symmetry axis (Fig. 4(b)). Growth can continue to form twelve twinned tetrahedra that share a common vertex with icosahedral symmetry or that grow disorderly. Interestingly, growth does not usually occur radially from this central particle with icosahedral symmetry. Instead most commonly first a tetrahedron is formed and gradually other tetrahedra arrange around it. In some instances, the system reorganizes and transforms into a single close-packed crystal at early stages, but in other trajectories icosahedral clusters survive to sizes comparable to the simulation box. Note that even in those cases in which the system crystallized into twinned tetrahedra the crystal grows from one single crystalline cluster but made of HCP and FCC particles. It would be interesting to perform simulations on larger systems to investigate the maximum size reached by these icosahedral structures.

Given that our analysis was performed over a limited number of trajectories (10 for each pressure) it is difficult to infer any trend in the propensity of the system to nucleate into twinned tetrahedra. Most of the trajectories adopt this structure at short times after the nucleation event, but only 20–30% are able to survive to large sizes.

These twinned FCC tetrahedra can be seen as incomplete Mackay icosahedra, a structure which is often found as the global energy minimum of finite size clusters in simple spherical models as Lennard-Jones.^{52–54} Inspired precisely by previous work on finite size clusters, we performed CNA of the twinned tetrahedra, which allowed us to clearly identify the five-fold axis and icosahedral centers in those structures (see Fig. 4(c)). The CNA signature of those environments is provided in Table 2. Growth into twinned tetrahedra is not a particularity of the PHS model, the same structures are also observed in the MD NVE simulations for HS. Indeed the appearance of these structures in the crystallization of HS has already been reported in previous work.^{55,56} Interestingly, it has been recently shown that HS colloids arrange into icosahedral clusters under spherical confinement.⁵⁷ In those conditions the free energy of icosahedral clusters is slightly lower than that of FCC ones up to at least $N = 4000$.

Finally, it is also interesting to mention that particles with both FCC and HCP environments are identified in all the trajectories, although there is a clear predominance of FCC over HCP particles. In general FCC particles are usually in the core of the nuclei whereas HCP particles are most commonly

found at the fluid–solid interface. For the HS model, the free energy of both solid phases is virtually the same, with the FCC solid being slightly more favourable.^{58–61} The preference of HS to crystallize in FCC environments has also already been noted in previous work.⁸

3.2 Hard-dumbbells with $L^* = 0.1, 0.2$ and 1

Given that PHD with elongations $L^* = 0.1, 0.2$ and 1 exhibit a similar crystallization behaviour, the results for these three cases will be described jointly here. Nucleation rates are gathered in Table 4, together with previous estimates from Ni and Dijkstra.²¹ Our results are consistent with previous data for HD with $L^* = 0.2$ and $L^* = 1$, with the nucleation rates for PHD being about an order of magnitude lower than that for HD at the same pressure. The reason for this small discrepancy might be attributed again to the slight softness of the spheres in the PHD, and it is likely that the results will come to a much closer agreement if the PHD were compared with HD using a scaled packing fraction as done in the previous section for PHS.

The evolution of density and the number of solid particles (see Fig. 6(a and b)) along the trajectories shows a similar behaviour to that found for PHS and HS, *i.e.* the density after the nucleation event does not always adopt the bulk density of the stable solid phase, remaining appreciably below it and in some instances undergoing a second jump after some time. Visual inspection of instantaneous configurations as well as analysis using the local order parameters described in Section 2 confirmed that, as seen in HS and PHS, the system often crystallizes into twinned tetrahedra sharing a common edge.

Table 4 Nucleation rates for PHD as obtained from NpT MD simulations as a function of elongation and pressure. The results for HD taken from ref. 21 (shown in bold) are also included for comparison. Nucleation rates are expressed in units of long diffusion times, $J^* = J\sigma_{\text{PHS}}^3\tau_D$

L^*	p^*	ρ^*	$\langle t^* \rangle$	D_t^*	J^*
0.1	17.75	1.029	63 465	6.3×10^{-3}	4.7×10^{-8}
0.1	18.00	1.032	15 882	5.9×10^{-3}	2.1×10^{-7}
0.1	18.25	1.035	10 773	5.6×10^{-3}	3.2×10^{-7}
0.1	18.50	1.038	5038	5.2×10^{-3}	7.3×10^{-7}
0.1	18.75	1.040	2136	4.9×10^{-3}	4.3×10^{-6}
0.2	22.00	1.071	51 853	4.4×10^{-3}	7.7×10^{-8}
0.2	22.25	1.073	34 628	4.2×10^{-3}	1.2×10^{-7}
0.2	22.50	1.075	7805	4.0×10^{-3}	5.7×10^{-7}
0.2	22.75	1.077	6626	3.9×10^{-3}	7.0×10^{-7}
0.2	23.00	1.079	2721	3.6×10^{-3}	1.9×10^{-6}
0.2	22.75			3.0×10^{-3}	4.4×10^{-6}
0.3	42.00	1.188	193 160	3.3×10^{-4}	2.7×10^{-7}
0.3	43.00	1.191	134 644	2.7×10^{-4}	4.8×10^{-7}
0.3	44.00	1.196	85 445	2.2×10^{-4}	9.2×10^{-7}
0.3	45.00	1.200	51 744	1.7×10^{-4}	2.0×10^{-6}
0.3	46.00	1.203	25 424	1.4×10^{-4}	5.1×10^{-6}
1.0	34.00			2.6×10^{-3}	7.3×10^{-7}
1.0	34.25	1.052	108 096	2.0×10^{-3}	5.1×10^{-8}
1.0	34.50	1.053	55 275	1.8×10^{-3}	1.1×10^{-7}
1.0	34.75	1.054	43 668	1.8×10^{-3}	1.5×10^{-7}
1.0	35.00	1.056	15 950	1.7×10^{-3}	4.0×10^{-7}
1.0	35.25	1.060	7019	1.7×10^{-3}	9.5×10^{-7}
1.0	35.50	1.061	4204	1.6×10^{-3}	1.7×10^{-6}

Table 5 Fraction of trajectories of PHD with $L^* = 0.3$ that spontaneously crystallized in each of the three identified solid phases

p^*	No. of runs	cP8	HCP PC	LD PC
42	10	0.20	0.80	0.00
43	20	0.25	0.65	0.15
44	10	0.40	0.30	0.30
45	20	0.50	0.30	0.20
46	10	0.20	0.40	0.40

At low elongations, the evolution of icosahedral clusters is completely analogous to that found in HS, *i.e.*, in some trajectories they transform quickly into a close-packed structure (see Fig. 6(c)), but in others twinned tetrahedra grow to quite large sizes (Fig. 6(d)). At $L^* = 1$, in contrast, the twinned tetrahedra usually grow disorderly until they almost fill the simulation box (Fig. 6(e)). Only a few trajectories crystallized in a layered close-packed solid. Regarding the type of solid environment, there are a large proportion of particles in both HCP and FCC environments, with a slight tendency to find a larger number of HCP particles. We can conclude that $L^* = 1$ exhibits the strongest propensity to form disordered twinned tetrahedral structures. The reason is probably related to the fact that a larger anisotropy leads to a slower diffusion of the particles. Especially once the twinned tetrahedra are formed, molecules are strongly constrained to their positions making a spontaneous reorganization of the particles into the aperiodic solid more difficult.

3.3 Hard-dumbbells with $L^* = 0.3$

The case of PHD with an elongation of $L^* = 0.3$ is particularly interesting. According to the phase diagram, the transition from the plastic to the orientationally ordered solid occurs at approximately $p^* = 43.15^{18}$ (see Fig. 1), which is within the crystallization range accessible to brute-force simulations ($p^* = 42–46$). Nucleation and growth of the orientationally ordered solid requires that particles find not only the right position but also the right orientation. In contrast, the formation of the plastic crystal only needs the particles to be at the right positions regardless of their orientation. Thus, it seems reasonable that nucleation of the plastic crystal is kinetically favoured even for pressures at which the orientationally ordered solid is the thermodynamically stable phase.

The nucleation rates for $L^* = 0.3$ are given in Table 4. As previously noted,²¹ at these intermediate elongations, dynamics becomes very slow, so that when the thermodynamic barrier for nucleation is low, crystallization is limited by the slow dynamics. As a result, crystallization by unbiased simulations requires rather long simulation times, which explains the absence of previous data at this level of supersaturation. As can be seen in Table 4, nucleation times are appreciably larger than those at lower and higher elongations at a similar degree of supersaturation. However, when expressed in terms of the time required for a particle to move a molecular diameter, the rates adopt similar values to that found at other elongations.

The evolution of the density along some representative trajectories is shown in Fig. 7(a). As in the previous cases,

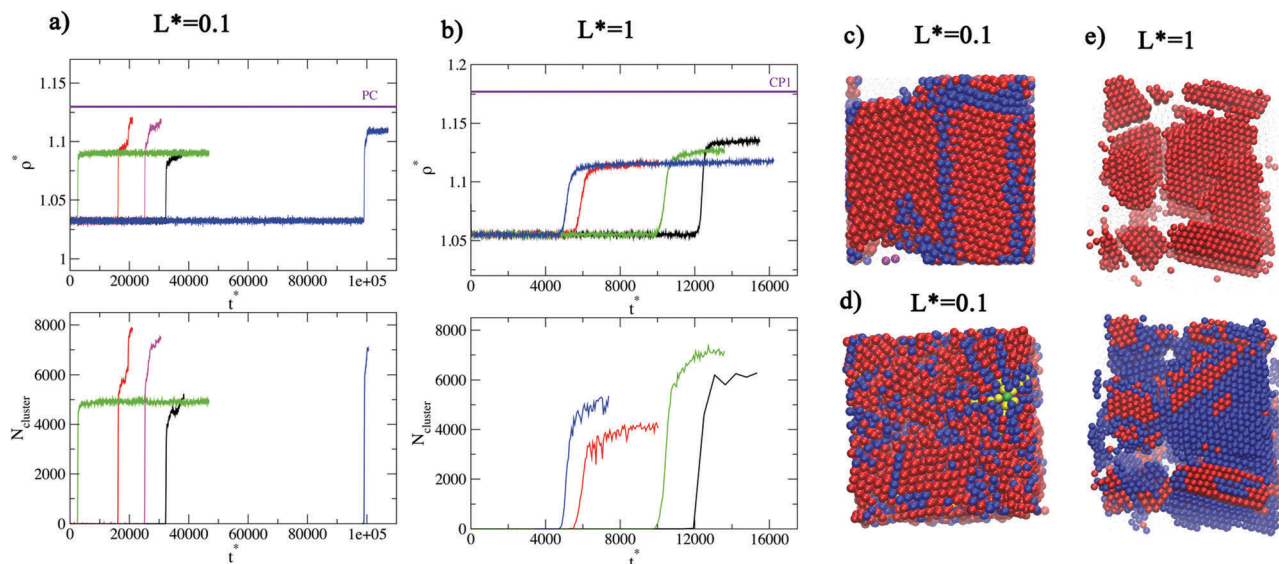


Fig. 6 (a and b) Evolution of the density along selected trajectories for $L^* = 0.1$ (a) and $L^* = 1$ (b). (c and d) Two examples of crystal growth at $L^* = 0.1$. Twinned tetrahedra are clearly visible in (d). (e) Typical icosahedral structure formed for PHD with $L^* = 1$. Particles are depicted in different colours depending on their environment: FCC are shown in red, HCP in blue, C5 axes in yellow and icosahedral centers in green. Particles are labelled using \bar{q}_6 and \bar{q}_4 parameters in (c) and (e) and using CNA (d).

nucleation is signaled by an abrupt increase of the density, but the equilibrium value after the jump does not always reach that of the stable solid phase. Depending on the behaviour of the density we identified three different scenarios: some trajectories equilibrated roughly at the density of the HCP or FCC PC, others somewhat below it and the remaining ones somewhat above it (Fig. 7(a) and 8). As can be seen in Fig. 8, even though there is some dispersion in the densities of the different structures associated with the presence of crystalline defects and incommensurability of the nucleated crystal with the simulation box, the structures formed can be classified according to their density. Note that always the equilibrium density is much lower than that of the orientationally ordered phase CP1. Only for those trajectories that equilibrated at the density of the PC, the jump was correlated to an abrupt increase in the number of solid particles identified with the Lechner and Dellago order parameter (see the middle panel of Fig. 7(a)). With the aim of getting insight into the crystallization behaviour, the emergent ordered structures were analyzed using a variety of strategies.

Let us start with those trajectories that equilibrated at the density of the PC. Visual inspection of the configuration (Fig. 7(b)) after the density jump, as well as comparison of the radial distribution function (Fig. 9(top panel)) with that of the PC solid, indicates the similarity between both structures. Analysis of the orientation order of the molecules using the probability distribution function (eqn (4), Fig. 10, bottom panel) evidences the plastic character of this solid. Thus we can conclude that the solid formed in these trajectories is a close-packed plastic crystal. Interestingly this occurred at pressures at which HCP PC is the thermodynamically stable phase ($p^* = 42, 43$) but also at those at which CP1 is more stable ($p^* = 44, 46$). These results confirm that the PC solid is

kinetically more accessible than the orientationally ordered solid as anticipated. Further analysis of the solid formed indicates that the close-packed structure crystallized from the fluid has hexagonal symmetry. The hexagonal arrangement of the centers of the molecules is confirmed both by the local bond order parameter \bar{q}_4 and by the BOOD (see Fig. 7(a and b)). This is consistent with the fact that HCP is more stable than FCC for HD with $L^* = 0.3$ (at these densities the chemical potential difference between the HCP and FCC PC is about $0.01-0.03Nk_B T^{20}$).

The case of the trajectories that equilibrate at densities above that of PC is particularly intriguing. Firstly, because the jump in density is not accompanied by an increase of number of solid particles as identified with the order parameter \bar{q}_6 , that is able to discriminate fluid from solid particles either in the PC or in the orientationally ordered solids (CP1, CP2 or CP3). But also because the density is somewhat higher than that of the PC but still too far away from that of the orientationally ordered solids (Fig. 7(a)). Both facts suggest that the crystal formed from the melt is not any of the solids found to be stable in the phase diagram of HD. This becomes evident when looking at the atomic configuration of the system after crystallization. Interestingly, the crystal formed in this case coincides with a stable phase of molecular nitrogen at high pressure, designated as $\delta\text{-N}_2^{62,63}$ and whose Pearson symbol⁶⁴ is cP16 if one looks at the positions of each nitrogen atom or cP8 if the molecular centers of mass are considered (see Fig. 7(c)). Note that molecular nitrogen presents a bond length of roughly $L^* = 0.3$. The structure of cP8 consists of a cubic-centred packing of edge sharing icosahedra, which is often found in binary alloys (such as Cr_3Si) and is also commonly referred as A15 Frank-Kasper phase.⁶⁵ The mechanical stability of this phase was assessed by generating a perfect lattice in which the centers of mass of the

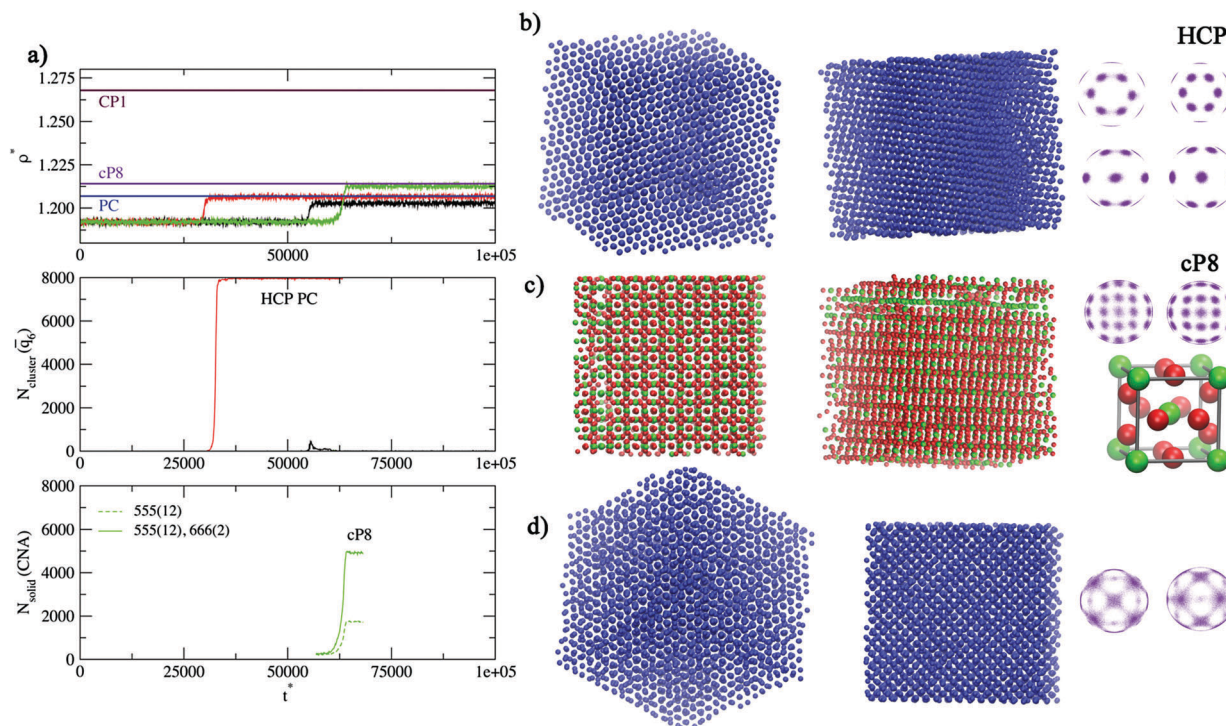


Fig. 7 (a) Evolution of the density (top panel), and number of particles in the largest solid cluster detected with the \bar{q}_6 order parameter (middle panel) and CNA (bottom panel) along three selected trajectories of PHD with $L^* = 0.3$ at $p^* = 43$. Of the three trajectories, in only one of them (red line) the jump in density is correlated with an increase of particles in the largest solid cluster as identified with the \bar{q}_6 order parameter. In this case the density after the jump matches quite closely that of the HCP PC (which is the stable phase at this p^*). The final configuration is depicted in (b) from two different views, together with its BOOD compared to that of the HCP PC. In the green trajectory the density after crystallization is higher than that of HCP PC and coincides with that of cP8 (δ -N₂ structure). \bar{q}_6 is unable to detect solid particles in this structure, but as shown in the bottom panel, the evolution of the number of solid particles can be monitored using CNA (the unit cell of cP8 comprises eight atoms, six with 555(12) and two with 555(12), 666(2) environments). Two different views of the final configuration and the unit cell are depicted in (c) with particles with the 555(12) environment coloured in green and particles with the 555(12), 666(2) environment shown in red. Finally, the trajectory shown in black is not able to reach the density of the HCP PC, staying slightly below it, and neither \bar{q}_6 nor CNA was able to discriminate solid from fluid particles. This structure designated as low-density plastic crystal is shown in (d) together with its BOOD.

dumbbells were arranged as in δ -N₂ (the unit cell was taken from ref. 66 and is depicted in Fig. 7(c)) and performing NpT simulations. This phase is mechanically stable over quite a broad range of pressures (Fig. 11). The equilibrium density after the jump (Fig. 7(a)) as well as the RDF (Fig. 9, middle panel) matches quite closely that of the simulations starting from a defect free cP8 structure. In the CP8 the molecules are able to rotate so that this phase is also a plastic crystal.

Given that the cP8 structure has a large degree of icosahedral order, it is not surprising that the usual order parameters based on spherical harmonics, such as the Lechner and Dellago order parameter used here, fail to discriminate fluid from solid particles. Simple fluids also tend to adopt local icosahedral environments at high densities. The similarity between the local environments of the fluid and solid phases is reflected in a large area of overlap in the \bar{q}_6 - \bar{q}_4 diagram (see Fig. 12). Even though CNA has known deficiencies identifying solid structures with small deviations of the bond distances from those in the perfect lattice, we found it useful to monitor the evolution of cP8 molecules during the crystallization simulations. cP8 has a cubic unit cell with eight atoms located at two types of lattice positions according to their local

environments, 6 atoms of which are surrounded by 12 nearest neighbours and the remaining two by 14 (see Fig. 7(c)). The CNA signatures of these two positions in a perfect cP8 structure are 555(12) and 555(12), 666(2). As can be seen in Fig. 7(a), analysis of the instantaneous configurations along the crystallization simulations reveals that the density jump indeed coincides with an abrupt increase of both types of environments, with a ratio of approximately 1/3. Regarding the molecular orientational order, calculation of the angular distribution function (eqn (4)) proves that the cP8 solid can be considered a plastic phase. Our simulations show that molecules located at 555(12), 666(2) positions have preferred orientations, whereas those with 555(12) are completely disordered. Precisely the same orientational behaviour has been reported also for δ -N₂.⁶⁷ Another similarity with nitrogen is that, in spite of the completely different structures of HCP and cP8 lattices, their densities are very similar, with cP8 being only about 0.5% more dense than HCP PC (δ -N₂ is 1% more dense than β -N₂ at the coexistence pressure at room temperature⁶⁷).

As far as we know previous evaluations of the phase diagram of HD did not consider the cP8 solid. So this phase might be thermodynamically stable for some range of pressures for

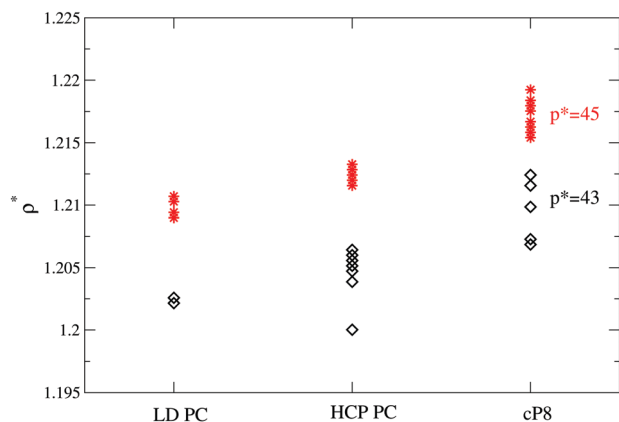


Fig. 8 Density of the final structures after the crystallization events for PHD with $L^* = 0.3$ at $\rho^* = 43$ (black diamonds) and $\rho^* = 45$ (red stars). There is a clear correlation between density and the crystal formed, with cP8 being the more dense, followed by HCP PC and the LD PC. Note that the density of all the competing crystal phases is rather similar, with differences between them lower than 1%. The dispersion of densities in the crystals formed with each structure is due to the presence of defects arising from incommensurability with the simulation box or from the rapid growth from the fluid.

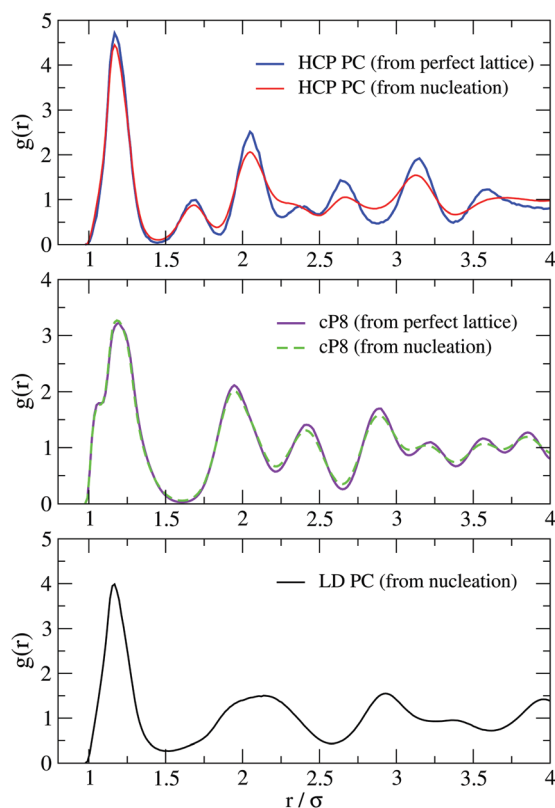


Fig. 9 Radial distribution functions of the HCP, cP8 and LD PC nucleated from the fluid for PHD with $L^* = 0.3$ at $\rho^* = 43$. The distributions of HCP and cP8 PC obtained from simulations starting from the perfect lattice are also shown for comparison.

dumbbells with $L^* = 0.3$. On the one hand, cP8 is slightly enthalpically favoured over HCP PC (due to its higher density)

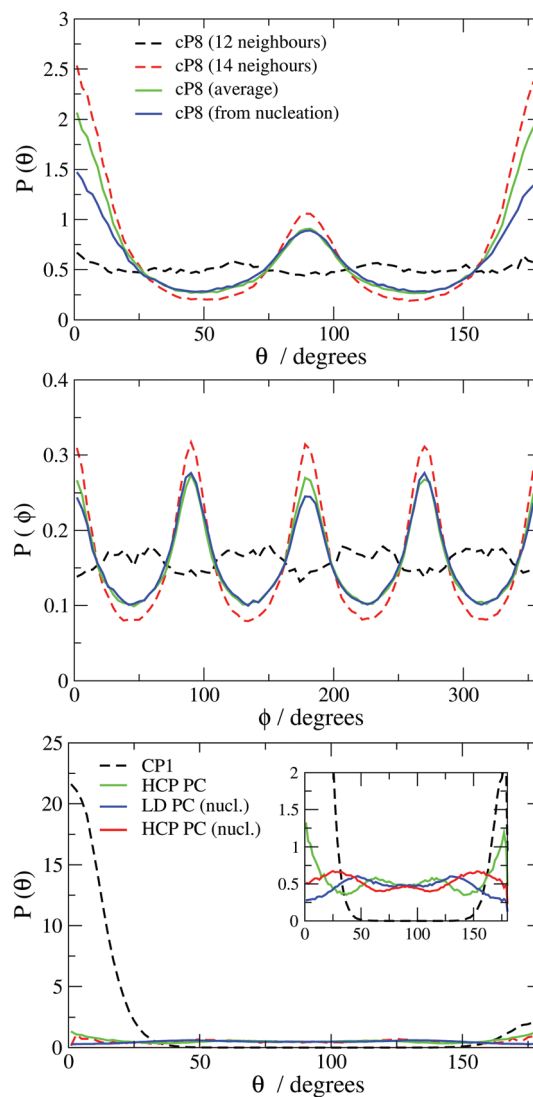


Fig. 10 Angular distribution functions of the cP8 (upper and middle panels), HCP and LD PC (lower panel) nucleated from the fluid for PHD with $L^* = 0.3$ at $\rho^* = 43$. The distributions of cP8, HCP PC and CP1 obtained from simulations starting from the perfect lattice are also shown for comparison.

but not over CP1. On the other hand, given that in cP8 1/4 of the particles show some orientational order, it might be somewhat entropically disfavoured with respect to PC but favoured over CP1. In summary, its thermodynamic stability will depend on a delicate balance between entropy and enthalpy and a definitive answer to this question can only be achieved from free energy calculations. Thus, we evaluated the free energy of the three competing phases using the Einstein molecule method,^{68–70} implemented in a home-made Monte Carlo code. The results are provided in Table 6. These data were used in conjunction with thermodynamic integration to calculate the phase transitions between them. We obtained that the transition FCC PC–CP1 occurs at a $p^* = 43.80(5)$ which is in reasonable agreement with the previous estimate of $p^* = 43.13$ of Vega *et al.*¹⁸ However, as already reported in the literature,

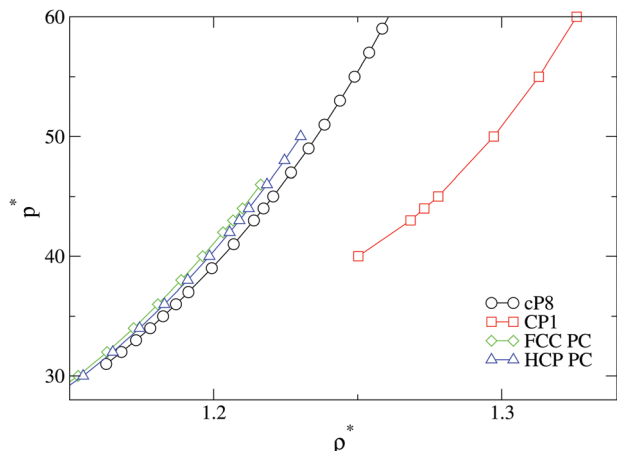


Fig. 11 Equation of state of the competing solid phases for PHD with $L^* = 0.3$.

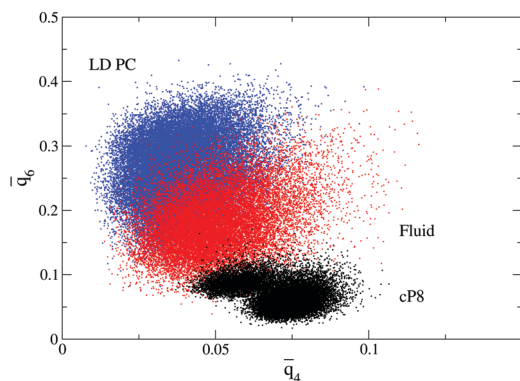


Fig. 12 \bar{q}_6 - \bar{q}_4 map for the fluid and for the cP8 and LD PC for dumbbells with $L^* = 0.3$ and $\rho^* = 43$. The large area of overlap between liquid and these phases makes these order parameters inadequate to accurately distinguish fluid from solid particles. In the case of cP8 this might be attributed to the fact that particles are arranged in environments with icosahedral symmetry, a local environment that is also often found in simple fluids at high densities.

the FCC PC is less stable than the HCP PC, with the coexistence of HCP PC and CP1 occurring at slightly higher pressure $p^* = 44.33(5)$. In contrast, the cP8-CP1 transition occurs at $p^* = 41.34(5)$, which means that cP8 is never the most stable phase for PHD with $L^* = 0.3$. Nevertheless, the chemical potential difference between cP8 and the most stable solid is within $0.13(5)k_B T$ in the range of pressures $p^* = 40$ -46, *i.e.* cP8 is only slightly metastable.

Finally, for those trajectories that equilibrate at densities below that of HCP PC, the increase in density is again not correlated with a sharp enhancement of solid particles as identified with the \bar{q}_6 order parameter. Similar to cP8, there is a large region of overlap between this structure and the fluid in the \bar{q}_6 - \bar{q}_4 map that makes these order parameters inadequate to discern fluid from solid particles (Fig. 12). Visual inspection of the structure indicates that it exhibits six-fold and four-fold symmetry axes (Fig. 7(d)). The radial distribution function coincides neither with those of the HCP or FCC PC nor with

Table 6 Free energies and coexistence pressures of the competing solid phases for PHD at $L^* = 0.3$. Note that free energies were not evaluated at the same pressure for all the solids. At $p^* = 43$ the free energy difference between cP8 and HCP PC is about $0.3Nk_B T$, but this difference is reduced to about $0.1Nk_B T$ when comparing the chemical potentials, due to the higher density of cP8

Phase	ρ^*	$A_{\text{tot}}/Nk_B T$
CP1	1.278	10.66(1)
FCC PC	1.160	7.42(1)
HCP PC	1.154	7.26(1)
cP8	1.158	8.42(1)

Coexisting phases	p_{coex}^*
FCC PC-CP1	43.80(10)
HCP PC-CP1	44.33(10)
cP8-CP1	41.34(10)

that of CP1 (Fig. 9, bottom panel). For example, the second peak at a distance of roughly 1.67σ in the RDF of HCP PC is absent in this crystal, which instead shows a rather broad second peak at a larger distance (coincident with the third peak of PC, and second and third peaks in the RDF of cP8). The crystalline character of this structure is evidenced by its diffraction pattern (Fig. 13) that exhibits Bragg peaks that indicate long range translational order and the BOOD (Fig. 7(c)) that shows ordering at the first coordination shell. Analysis of the angular distribution function indicates that molecules are not orientationally ordered. Given that this structure has a density slightly lower than that of HCP PC, in what follows, it will be designated low density plastic crystal (LD PC). We have been unable to infer the unit cell of this structure, which does not seem to be one of the stable phases of nitrogen as HCP and cP8 solids. However, we would like to highlight the difficulty of identifying solid structures, as crystals with very similar densities such as HCP and cP8 can have disparate unit cells with radically different molecular arrangements.

The number of trajectories following each path as a function of pressure is given in Table 5. Even though the number of simulations performed at each pressure is rather limited (10 at $p^* = 42, 44$, and 46, and 20 at $p^* = 43$ and 45), some clear trends can be inferred. For example, cP8 appears more frequently as pressure increases, reaching a maximum at $p^* = 45$ to decrease

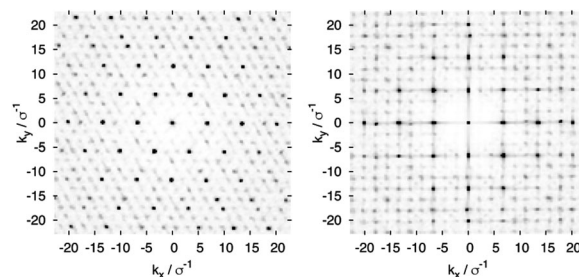


Fig. 13 Diffraction pattern of the LD PC formed from the melt of PHD with $L^* = 0.3$ at $\rho^* = 43$ measured along the four-fold (right figure) and six-fold (left figure) symmetry axes. Bragg peaks are clearly visible that corroborate the crystalline character of this structure.

again at $p^* = 46$. Similarly, the probability of forming the LD PC remains rather constant at $p^* = 43$ –45 but in this case the maximum probability is found at $p^* = 46$. Note that at $p^* = 42$ –44, HCP PC is the most stable phase, but at $p^* = 45$ –46 CP1, which has never been spontaneously formed in the crystallization simulations, is the most stable phase. Our observations can be rationalized with Ostwald³⁰ and Stranski and Totomanow³² suggestions that the phase that crystallizes first is not the most stable one but that separated from the fluid by a lower free energy barrier. Given the frequency of formation of the three solid structures, we can conclude that their nucleation barriers differ only by about 1 – $2k_B T$, *i.e.*, there is a strong competition between these three solid phases. In contrast, the nucleation barrier of CP1 must be considerably higher than those of these three competing phases.

Regarding the growth mechanism, the evolution of the solid nucleus of HCP and cP8 PC is shown in Fig. 14. In spite of the large structural differences between both phases, the growth mechanism is completely analogous. A rather spherical nucleus with the same structure as the final crystal forms and grows gradually without the presence of intermediate structural transformations.

3.4 Nucleation barriers

As mentioned in Section 2, brute force simulations do not provide a direct way to measure the free energy barrier for nucleation.

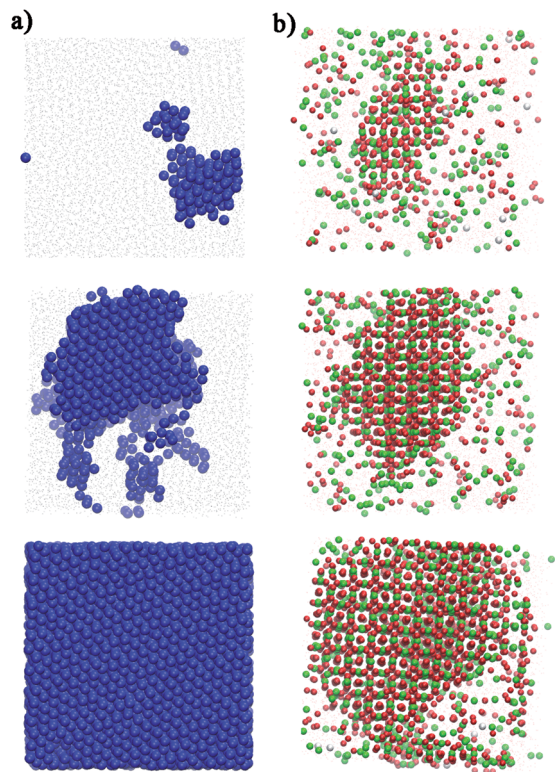


Fig. 14 Growth of the crystal along two representative trajectories of PHD with $L^* = 0.3$ at $p^* = 43$. In (a) the fluid crystallizes into a HCP solid (particles with an HCP environment are shown in blue) and in (b) the fluid transforms into a cP8 solid (particles with twelve neighbours are shown in green and particles with fourteen neighbours in red).

Table 7 Approximate estimates of free energy barriers for nucleation for PHS and PHD at different elongations

L^*	p^*	ρ^*	N_c	$\Delta\mu$ ($k_B T$)	λ/σ	ΔG ($k_B T$)
0	17.00	1.024	10	0.53	0.33	19(2)
0.2	22.00	1.071	80	0.46	0.33	19(2)
0.2	22.75	1.077	50	0.53	0.33	16(2)
0.3	42.00	1.118	50	0.45	0.33	17(2)
0.3	46.00	1.203	50	0.54	0.33	15(2)
1.0	34.25	1.052	10	0.54	0.33	18(2)

However, we can use eqn (2) to get a rough estimate. Besides nucleation rates, we need to know the number of particles in the critical nucleus, the difference of chemical potential between the solid and the fluid and the λ parameter. A very rough estimation of the number of particles in the critical nucleus was obtained by looking at the evolution of the number of particles in the largest cluster. Note that a more precise estimate can be obtained from a more detailed analysis,⁷¹ although, even doing so, this property is inherently ambiguously defined, as it is rather sensitive to the order parameter used to distinguish fluid from solid particles.⁶ Our estimates of N_c are somewhat lower than those of Ni and Dijkstra (see Table 7), which we attribute precisely to the use of a different (more stringent for a particle to be considered solid-like) order parameter. $\Delta\mu$ can be obtained by thermodynamic integration from the melting point. For $L^* = 1$, $\Delta\mu$ was taken from ref. 21. For $L^* = 0.2$ and $L^* = 0.3$, $\Delta\mu$ was estimated by thermodynamic integration from the fluid–PC coexistence point, which was obtained by performing free energy calculations and looking for the pressure at which the chemical potential of both phases is equal. Using this procedure we obtained that the fluid–PC transition occurs at $p^* = 24.87$ for $L^* = 0.2$ and at $p^* = 24.87$ for $L^* = 0.3$. For $L^* = 0$, $\Delta\mu$ was also obtained from thermodynamic integration from the coexistence point, which was taken from ref. 34. Previous work has found that $\lambda = 0.33$ for PHS.³⁸ Estimates of λ for HD using the attachment rates given in ref. 21 indicate that λ is roughly constant with L^* and adopts values between 0.14 and 0.20. Thus we have decided to use the same value of $\lambda = 0.33$ for all systems. The approximate values of the free energy barriers for nucleation are given in Table 7. Given all the approximations used, the error in the free energy barriers is probably about $2k_B T$. In any case, our results are rather consistent with those of Ni and Dijkstra.²¹ Note that for $L^* = 0.3$, even though three different polymorphs are competing, we only calculated one free energy barrier taking into account all the trajectories. As mentioned before, given the frequency of appearance, differences between the three polymorphs are of the order of only 1 – $2k_B T$, which is of the order of our error. From these results it can be concluded that spontaneous nucleation for PHD is accessible on typical time-scales of MD simulations when the nucleation barrier is of the order of 15 – $19k_B T$.

4 Conclusions and outlook

In this work we have investigated the crystal nucleation of pseudo-hard spheres and dumbbells at moderate metastability using brute force simulations. The nucleation rates obtained

for PHS and PHD are consistent with those previously reported for HS and HD, being about an order of magnitude larger in the PHS and PHD models than in HS and HD at the same elongation and pressure. This is hardly surprising as the pseudo-hard sphere model is known to reproduce quite closely many properties of the hard-sphere model, such as, for example, the density of the liquid and solid phases,³³ the coexistence pressure³⁸ or the diffusion constant.³⁵ Thus it seems intuitive that PHD would also behave similarly to HD.

Analysis of the structures formed in the crystallization simulations of PHS ($L^* = 0$) and PHD with short ($L^* = 0.1$ and 0.2) and large ($L^* = 1$) elongations reveals that quite often the fluid organizes into an ordered structure in which a large proportion of molecules are identified as solid but are arranged into tetrahedra sharing a common vertex, as in a Mackay icosahedron. This kind of structures had already been reported for HS.^{55,56} Given the similarity in the crystal growth between HS and PHS, it seems likely that the twinned tetrahedra found in PHD also appear in HD. Curiously, a similar growth pattern has been reported for the coarse-grained mW model of water (in which water is modelled as a spherical particle with three-body terms), although in this case the twinned tetrahedra are made of cubic and hexagonal diamond local arrangements.⁷²

PHD with intermediate elongation $L^* = 0.3$ exhibit a completely different behaviour. In this case we do not observe the formation of twinned tetrahedra. Instead the fluid can freeze into three plastic solids, namely, HCP, cP8 and LD PC, with rather different structures but with densities within 0.5%. At the lower studied pressures ($p^* = 42$ – 44) the HCP PC is the most stable phase, but at high pressures ($p^* = 44$ – 46) the orientationally ordered solid CP1, which has never been found in our crystallization simulations, is more stable. Consistent with the Ostwald rule,³⁰ the solid that crystallizes first does not always coincide with the most stable phase, but with that separated from the fluid by a lower energy barrier. Given that the probability of finding the three plastic crystals differs by a maximum factor of 2–3 in the range of pressures considered, it can be concluded that the nucleation free energy barriers are within 1 – $2k_B T$ for the three structures. We have also seen that the free energies of HCP and cP8 are very similar within this range of pressures, indicating that they are almost degenerate. It is surprising to find the ability of this system to arrange in three very different structures but with rather similar thermodynamic properties (similar density, free energy and barrier to the fluid phase). The nucleation barrier of CP1, in contrast, must be appreciably higher than that of the three competing plastic solids, which we attribute to the fact that dumbbells need to find at the same time the right position and orientation in order to nucleate CP1. Given the high density and low diffusion of the system at these high pressures, such a large rearrangement of the particles directly from the fluid phase is probably the cause of a high nucleation free energy barrier.

The results at intermediate elongations are of relevance to molecular nitrogen. Indeed β -N₂ (stable under room conditions) and δ -N₂ (stable at high pressure⁶²) are structurally identical to the competing HCP and cP8 plastic crystals. Curiously, studies of

nucleation of the plastic phase β -N₂ using more realistic models of molecular nitrogen describe a two step mechanism in which an orientationally ordered structure forms first that then evolves to the stable plastic phase (β -N₂).^{73,74} We have never observed this nucleation mechanism in our simulations. It is likely that the attractive energy between molecules in the model used to describe N₂ favours the alignment of nitrogen molecules, favouring the formation of an orientationally ordered solid. In spite of the obvious differences between the behaviour of dumbbells and real molecular nitrogen, the ability of dumbbells to form a large number of structures found in real nitrogen, even if they are metastable for dumbbells, is remarkable.

In summary, our study shows that nucleation of simple models introducing anisotropy can exhibit a complex nucleation behaviour. The presence of several polymorphs with similar nucleation free energy barriers and stability can lead to a very rich nucleation behaviour with the crystallization of the competing phases with similar probabilities. In future work it would be interesting to extend the study of nucleation of dumbbells with $L^* = 0.3$ at lower supersaturations and at slightly lower and larger elongations. Given the similarity of the densities and nucleation free energy barriers of the competing HCP, cP8 and LD PC, it is possible that slight changes in pressure or elongation might favour the formation of one structure over the others. Indeed, given the similar chemical potential of HCP and cP8 PC, it is even possible that cP8 might be thermodynamically stable for some range of elongations. Obviously it would also be interesting to get further insight into the structure of the LD PC and find an order parameter that allows its identification. In particular, it would be of relevance to assess its thermodynamic stability with respect to the other competing solid phases. As mentioned in the Introduction, crystallization at elongations around $L^* = 0.9$ is also likely to be interesting. In that case, there might be a competition between the random packed structure and the orientationally ordered solid CP1. Again, intuitively, one would think that the random close packed structure might be more accessible than the stable CP1 phase at high pressure.

Our findings are also of relevance to colloidal science. We have found that simple dimer colloids can arrange into rather complex structures such as cP8 and LD PC, which even if metastable, can be accessed from the fluid under appropriate thermodynamic conditions.

Conflicts of interest

There are no conflicts to declare.

Acknowledgements

IZ was supported by a Garantía Juvenil contract from CSIC (with FEDER funds). This work was also funded by the Agencia Estatal de Investigación and the Fondo Europeo de Desarrollo Regional (FEDER) under Grant No. FIS2015-72946-EXP(AEI), FIS2017-89361-C3-2-P(AEI/FEDER,UE) and FIS2016-78117-P.

Useful discussions with Jon Doye, Lourdes Infantes, Enrique Lomba, Eduardo Sanz and Jorge Espinosa are gratefully acknowledged.

References

- G. C. Sosso, J. Chen, S. J. Cox, M. Filtzner, P. Pedevilla, A. Zen and A. Michaelides, *Chem. Rev.*, 2016, **116**, 7078.
- B. J. Alder and T. E. Wainwright, *J. Chem. Phys.*, 1957, **27**, 1208–1209.
- W. W. Wood and J. D. Jacobson, *J. Chem. Phys.*, 1957, **27**, 1207–1208.
- P. N. Pusey and W. van Megen, *Nature*, 1986, **320**, 340.
- S. Auer and D. Frenkel, *Nature*, 2001, **409**, 1020–1023.
- L. Filion, M. Hermes, R. Ni and M. Dijkstra, *J. Chem. Phys.*, 2010, **133**, 244115.
- T. Kawasaki and H. Tanaka, *PNAS*, 2010, **107**, 14036.
- L. Filion, R. Ni, D. Frenkel and M. Dijkstra, *J. Chem. Phys.*, 2011, **134**, 134901.
- M. Radu and T. Schilling, *EPL*, 2014, **105**, 2.
- T. Schilling, H. J. Schope, M. Oettel, G. Opletal and I. Snook, *Phys. Rev. Lett.*, 2010, **105**, 025701.
- J. T. Berryman, M. Anwar, S. Dorosz and T. Schilling, *J. Chem. Phys.*, 2016, **145**, 211901.
- M. Leocmach and H. Tanaka, *Nat. Commun.*, 2012, **3**, 974.
- J. Russo and H. Tanaka, *Sci. Rep.*, 2012, **2**, 505.
- T. Schilling and D. Frenkel, *Comput. Phys. Commun.*, 2005, **169**, 117–121.
- A. Cuetos and M. Dijkstra, *Phys. Rev. Lett.*, 2007, **98**, 905701.
- R. Ni, S. Belli, R. van Roij and M. Dijkstra, *Phys. Rev. Lett.*, 2010, **105**, 088302.
- C. Vega, E. P. A. Paras and P. A. Monson, *J. Chem. Phys.*, 1992, **96**, 9060.
- C. Vega, E. P. A. Paras and P. A. Monson, *J. Chem. Phys.*, 1992, **97**, 8543.
- C. Vega and P. A. Monson, *J. Chem. Phys.*, 1997, **107**, 2696.
- M. Marechal and M. Dijkstra, *Phys. Rev. E: Stat., Nonlinear, Soft Matter Phys.*, 2008, **77**, 061405.
- R. Ni and M. Dijkstra, *J. Chem. Phys.*, 2011, **134**, 034501.
- P. M. Johnson, C. M. van Kats and A. van Blaaderen, *Langmuir*, 2005, **21**, 11510–11517.
- A. F. Demirors, P. M. Johnson, C. M. van Kats, A. van Blaaderen and A. Imhof, *Langmuir*, 2010, **26**, 14466–14471.
- J. D. Forster, J.-G. Park, M. Mittal, H. Noh, C. F. Schreck, C. S. O'Hern, H. Cao, E. M. Furst and E. R. Dufresne, *ACS Nano*, 2011, **5**, 6695–6700.
- F. Tu, B. J. Park and D. Lee, *Langmuir*, 2013, **29**, 126979.
- A. S. Stender, X. Wei, A. E. Augspurger and N. Fang, *J. Phys. Chem. C*, 2013, **117**, 16195–16202.
- B. Peng, H. R. Vutukuri, A. van Blaaderen and A. Imhof, *J. Mater. Chem.*, 2012, **22**, 21893–21900.
- F. Chu, N. Heptner, Y. Lu, M. Siebenburger, P. Lindner, J. Dzubiella and M. Ballauff, *Langmuir*, 2015, **31**, 5992–6000.
- J. R. Wolters, J. E. Verweij, G. Avvisati, M. Dijkstra and W. K. Kegels, *Langmuir*, 2017, **33**, 3270–3280.
- W. Ostwald, *Z. Phys. Chem.*, 1897, **22**, 286.
- K. F. Kelton, *Crystal nucleation in liquids and glasses*, Academic, Boston, 1991.
- I. N. Stranski and D. Totomanow, *Z. Phys. Chem.*, 1933, **399**, 163.
- J. Jover, A. J. Haslam, A. Galindo, G. Jackson and E. A. Müller, *J. Chem. Phys.*, 2012, **137**, 144505.
- J. R. Espinosa, E. Sanz, C. Valeriani and C. Vega, *J. Chem. Phys.*, 2013, **139**, 144502.
- P. Rosales-Pelaez, P. M. de Hijes, E. Sanz and C. Valeriani, *J. Stat. Mech.: Theory Exp.*, 2016, **9**, 094005.
- E. Lindahl, B. Hess and D. van der Spoel, *J. Mol. Model.*, 2001, **7**, 306–317.
- M. J. Abraham, T. Murtol, R. Schulz, S. Pall, J. C. Smith, B. Hess and E. Lindahl, *SoftwareX*, 2015, **1–2**, 19–25.
- J. R. Espinosa, C. Vega, C. Valeriani and E. Sanz, *J. Chem. Phys.*, 2016, **144**, 034501.
- G. Bussi, D. Donadio and M. Parrinello, *J. Chem. Phys.*, 2007, **126**, 014101.
- M. Parrinello and A. Rahman, *J. Appl. Phys.*, 1981, **52**, 7182–7190.
- M. P. Allen and D. J. Tildesley, *Computer Simulation of Liquids*, Oxford Science Publications, Oxford, 2004.
- K. R. Hall, *J. Chem. Phys.*, 1972, **57**, 2252.
- W. Lechner and C. Dellago, *J. Chem. Phys.*, 2008, **129**, 114707.
- D. C. Rapaport, *The Art of Molecular Dynamics Simulation*, Cambridge University Press, Cambridge, 2004.
- J. R. Espinosa, C. Navarro, E. Sanz, C. Valeriani and C. Vega, *J. Chem. Phys.*, 2016, **145**, 211922.
- D. Faken and H. Jonsson, *Comput. Mater. Sci.*, 1994, **2**, 279–286.
- A. Stukowski, *Modell. Simul. Mater. Sci. Eng.*, 2012, **20**, 045021.
- P. J. Steinhardt, D. R. Nelson and M. Ronchetti, *Phys. Rev. B: Condens. Matter Mater. Phys.*, 1983, **28**, 784.
- T. Schilling, S. Dorosz, H. J. Schope and G. Opetal, *J. Phys.: Condens. Matter*, 2011, **23**, 194120.
- S. Auer, W. C. K. Poon and D. Frenkel, *Phys. Rev. E: Stat., Nonlinear, Soft Matter Phys.*, 2003, **67**, 020401.
- E. G. Noya, C. Vega and E. de Miguel, *J. Chem. Phys.*, 2008, **128**, 154507.
- A. Northby, *J. Chem. Phys.*, 1987, **87**, 6166.
- D. Wales and J. P. K. Doye, *J. Phys. Chem. A*, 1997, **101**, 511.
- Y. H. Xiang, H. Jiang, W. S. Cai and X. G. Shao, *J. Phys. Chem. A*, 2004, **108**, 3586.
- B. O'Malley and I. Snook, *Phys. Rev. Lett.*, 2003, **8**, 085702.
- N. C. Karayiannis, R. Malshe, M. Kroger, J. J. de Pablo and M. Laso, *Soft Matter*, 2012, **8**, 844.
- B. de Nijs, S. Dussi, F. Smalenburg, J. D. Meeldijk, D. J. Groenendijk, L. Filion, A. Imhof, A. van Blaaderen and M. Dijkstra, *Nat. Mater.*, 2015, **14**, 56.
- P. G. Bolhuis, D. Frenkel, S.-C. Mau and D. A. Huse, *Nature*, 1997, **388**, 235.
- L. V. Woodcock, *Nature*, 1997, **388**, 236.
- S.-C. Mau and D. A. Huse, *Phys. Rev. E: Stat. Phys., Plasmas, Fluids, Relat. Interdiscip. Top.*, 1999, **59**, 4396.
- E. G. Noya and N. Almarza, *Mol. Phys.*, 2015, **113**, 1061–1068.

- 62 A. F. Schuch and R. L. Mills, *J. Chem. Phys.*, 1970, **52**, 6000.
- 63 D. T. Cromer, R. L. Mills, D. Schiferl and L. A. Schwalbe, *Acta Crystallogr., Sect. B: Struct. Crystallogr. Cryst. Chem.*, 1981, **37**, 8–11.
- 64 Pearson symbol is a notation used in crystallography to describe crystal structures consisting on two letters and a number. The first letter indicates the crystal family, the second one the centering type, followed by the number of atoms in the unit cell.
- 65 F. C. Frank and J. S. Kasper, *Acta Crystallogr.*, 1959, **12**, 483.
- 66 Inorganic Crystal Structure Database (ICSD), http://www2.fiz-karlsruhe.de/icsd_home.html.
- 67 R. L. Mills, B. Olinger and D. T. Cromer, *J. Chem. Phys.*, 1986, **84**, 2837.
- 68 D. Frenkel and A. J. C. Ladd, *J. Chem. Phys.*, 1984, **81**, 3188–3193.
- 69 C. Vega and E. G. Noya, *J. Chem. Phys.*, 2007, **127**, 154113.
- 70 E. G. Noya, M. M. Conde and C. Vega, *J. Chem. Phys.*, 2008, **128**, 154507.
- 71 J. Wedekind, R. Strey and D. Reguera, *J. Chem. Phys.*, 2007, **126**, 134103.
- 72 T. Li, D. Donadio, G. Russo and G. Galli, *Phys. Chem. Chem. Phys.*, 2011, **13**, 19807.
- 73 J.-M. Leyssale, J. Delhommelle and C. Millot, *Chem. Phys. Lett.*, 2003, **375**, 612.
- 74 J.-M. Leyssale, J. Delhommelle and C. Millot, *J. Chem. Phys.*, 2005, **122**, 104510.